Title
NMR Spectroscopy Reveals Adsorbate Binding Sites in the Metal–Organic Framework UiO-66(Zr)

Journal
The Journal of Physical Chemistry C, 122(15)

ISSN
1932-7447

Authors
Nandy, Aditya
Forse, Alexander C
Witherspoon, Velencia J
et al.

Publication Date
2018-04-19

DOI
10.1021/acs.jpcc.7b12628

Peer reviewed

THE JOURNAL OF PHYSICAL CHEMISTRY C

Article

Cite This: J. Phys. Chem. C XXXX, XXX, XXX−XXX

pubs.acs.org/JPCC

NMR Spectroscopy Reveals Adsorbate Binding Sites in the Metal−Organic Framework UiO-66(Zr)

Aditya Nandy,[†] Alexander C. Forse,[†,‡,∥] Velencia J. Witherspoon,[*,†,⊥] and Jeffrey A. Reimer[*,†,§,⊥]

[†]Department of Chemical and Biomolecular Engineering, University of California, Berkeley, Berkeley, California 94720, United States

[‡]Department of Chemistry, University of California, Berkeley, Berkeley, California 94720, United States

[§]Materials Science Division, Lawrence Berkeley National Laboratory, Berkeley, California 94720, United States

[∥]Berkeley Energy and Climate Institute, University of California, Berkeley, Berkeley, California 94720, United States

Supporting Information

ABSTRACT: We assign ^{1}H and ^{13}C NMR resonances emanating from acetone, methanol, and cyclohexane adsorbed inside the pores of UiO-66(Zr). These results are informed by density functional theory (DFT) calculations, which probe the role of two competing effects inside of the pore environment: (i) nucleus independent chemical shifts (NICSs) generated by ring currents in conjugated linkers and (ii) small molecule coordination to the metal-oxyhydroxy cluster. These interactions are found to perturb the chemical shift of in-pore adsorbate relative to ex-pore adsorbate (which resides in spaces between the MOF particles). Changes in self-solvation upon adsorption may also perturb the chemical shift. Our results indicate that cyclohexane preferentially adsorbs in the tetrahedral pores of UiO-66(Zr), while acetone and methanol adsorb at the Zr−OH moieties on the metal-oxyhydroxy clusters in a more complex fashion. This method may be used to probe molecular adsorption sites and material void saturation with selected adsorbates, and with further development may eventually be used to trace in-pore chemistry of MOF materials.

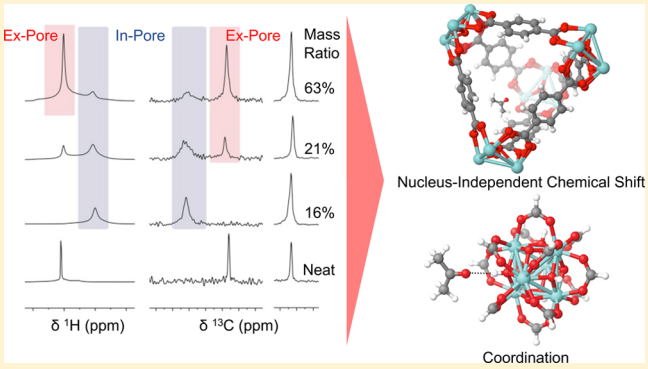

INTRODUCTION

For the last two decades, metal−organic frameworks (MOFs) have been a topic of investigation due to their high surface areas, tunable structures, and modular linker chemistries.[1,2] These systematically variable properties have allowed MOFs to be employed for a variety of purposes, from chemical storage[3,4] and separations[5] to heterogeneous catalysis.[6] The periodic nature of MOFs, comprised of organic linkers connecting inorganic metal-oxyhydroxy clusters, presents extraordinary chemical design opportunities and synthetic challenges.

The UiO family of MOFs is of particular interest due to its high thermal and chemical stability,[7] as well as its potential for industrial use due to facile and scalable synthesis.[8−10] UiO-66(Zr) is a face-centered cubic MOF that contains tetrahedral and octahedral pores, as illustrated in Figure 1. These pores arise from the voids created by terephthalic acid linkers connecting Zr-based metal-oxyhydroxy clusters ($Zr_6O_4(OH)_4$). This family of frameworks has demonstrated reverse shape selectivity in liquid separations,[11,12] suggesting the importance of improving the understanding of cage environments to enhance separation properties. Recent investigations have revealed that key characteristics of these frameworks (such as functionalization of the organic linkers,[13,14] variation of the inorganic cluster,[15,16] crystallite size,[17] and presence of missing-linker defects[18−20]) greatly affect the material performance, including chemical storage and catalysis.[21−24] Fewer studies, however, trace in-pore adsorbate chemistries within MOFs, in part due to the challenge of differentiating between in- and ex-pore adsorbates with common spectroscopies.

Correlating the influence of differing MOF pore environments on adsorbate molecular dynamics is essential for improving MOF design practices and grasping the nature of adsorbate−adsorbent interactions. To this end, quasi-elastic neutron scattering (QENS) and molecular dynamics (MD) simulations have been used in a complementary fashion to measure and interpret the self-diffusion coefficients of guest molecules in UiO-66(Zr), which were found to be very small (10^{-11} m^2 g^{-1}).[25,26] In other studies, ^{129}Xe NMR and MD simulations were successfully employed to determine xenon dynamics in the UiO family of frameworks with varying cage sizes.[27] Separately, NMR relaxometry measurements have quantified the relative distributions of adsorbates in nanometer-sized MOF pores (in-pore) and micrometer-sized voids (ex-pore) of various MOFs, illustrating the potential for NMR methods to differentiate adsorbate environments.[28] Establishing accessible spectroscopic methods (void of complex analysis) to

Received: December 22, 2017
Revised: February 27, 2018
Published: March 23, 2018

DOI: 10.1021/acs.jpcc.7b12628
J. Phys. Chem. C XXXX, XXX, XXX−XXX

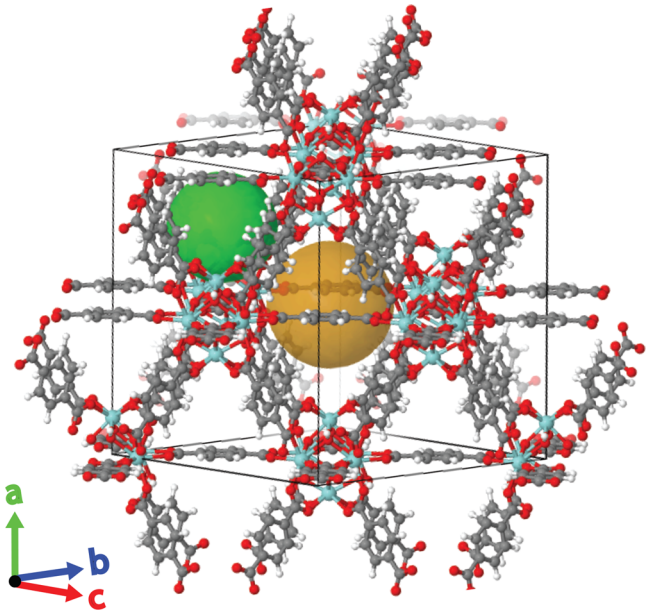

Figure 1. Unit cell (black outline) of UiO-66(Zr) consisting of the metal-oxyhydroxy cluster and terephthalate linkers.[16] Zirconium (blue), oxygen (red), carbon (gray), and hydrogen (white) constitute the full structure. Green and orange spheres represent the tetrahedral and octahedral pores, respectively.

probe in-pore species would enable the utilization of NMR for real-time monitoring of processes involving adsorbed small molecules. Adsorbed molecules can be distinguished by interactions taking place in differentiated in-pore MOF environments. Developing pore-type specific structure–property relationships in MOFs with diversified pores will ultimately lead to more efficient separations and catalysis with MOFs.

Investigations of other porous materials with conjugated π-electron systems, such as activated carbons[29−31] and carbon nanotubes,[32] have shown that in- and ex-pore guest molecules are identifiable based on distinct chemical shifts that arise from local magnetic fields generated by ring currents in the host system.[33] In these systems, in-pore adsorbate experiences a nucleus independent chemical shift (NICS),[34] which can be obtained from DFT calculations as a function of position by employing the Biot–Savart law.[32,35] In many experiments on adsorbed molecules in porous carbons, similar chemical shift deviations ($\Delta\delta$) are observed for different atoms (including ^{1}H and second period elements such as ^{31}P/^{19}F).[36,37] However, in some cases for heavy atoms, different shift deviations may be observed due to polarizability.[32] In addition to the NICS, local interactions can have an impact on chemical shift deviations. Extensive experimental work corroborated by DFT calculations have demonstrated the impact of weak local interactions (i.e., hydrogen bonding) on the proton chemical shift.[38,39] Furthermore, local interactions have been investigated in the context of crystal packing effects on a guest molecule, with the host acting as a "tweezer," providing a distinct short-range electronic environment sampled by the guest. In these crystal packing studies, nuclei other than protons were found to have chemical shift deviations with many contributing factors, including long-range NICS effects and local currents arising from packing.[40] The abundance of conjugated aromatic rings in MOF linkers motivated us to explore the suitability of NICS quantification in MOFs as a means to study molecular adsorption. In fact, previous NMR studies[41] of alkanes in UiO-67 demonstrate a negative chemical shift of in-pore adsorbed light alkanes relative to the free gases, which could be explained by NICSs.[42−45]

The present work examines the adsorption of small molecule adsorbates in UiO-66(Zr) with NMR spectroscopy and is informed by DFT calculations. In- and ex-pore chemical shift(s) are differentiated by increasing the adsorbate loading past saturation, where the ex-pore environment is easily identifiable. The nature of the adsorbate is varied to probe consistency of ring current effects on the adsorbate chemical shifts. We present DFT calculations that inform possible reasons for the differences in chemical shifts between the in- and ex-pore adsorbate molecules. Adsorbate molecules that do not interact chemically with the adsorbent present NICS changes, whereas adsorbates with adsorbent-specific intermolecular interactions (e.g., oxygen-assisted hydrogen bonding) have chemical shift deviations in different directions for different nuclei. We conclude that NICS due to organic linker ring currents dominate the observed chemical shifts for adsorbates when there are no chemically specific adsorbent–adsorbate interactions. Our work enables determination of the preferred adsorption sites in UiO-66(Zr) and should be applicable to other MOFs.

EXPERIMENTAL AND THEORETICAL METHODS

Synthesis. UiO-66(Zr) was synthesized following a previously reported procedure for UiO-66(Hf), with $ZrCl_4$ in place of $HfCl_4$.[46] In this bulk synthesis procedure, 0.35 g (1.5 mmol) of $ZrCl_4$ (Sigma, 99+%) and 0.25 g (1.5 mmol) of 1,4-benzenedicarboxylic acid (H_2BDC) (Sigma, 98%) were dissolved in 20 mL of DMF (Fisher Scientific, 99+%) in a Schott bottle (100 mL volume). Ten milliliters of formic acid (Sigma, 95%) was added as a modulator (after dissolution of the reactants) to increase both crystallinity and yield.[47] An airtight Schott bottle cap was found to be important for a successful solvothermal synthesis. The bottle was sealed and heated to 393 K for 24 h. UiO-66(Zr) was then recovered via vacuum filtration.

Activation. Newly synthesized UiO-66(Zr) was activated as reported previously.[14,48] The material was washed with DMF three times to rid any residual reactant. After undergoing four solvent exchanges with methanol to remove DMF, the UiO-66(Zr) material was filtered, dried, and evacuated under vacuum at 378 K for 12 h.

Characterization. Powder X-ray diffraction (PXRD) data was obtained with a Bruker D8 Discover GADDS Powder X-ray diffractometer with Cu Kα radiation (λ = 1.540 Å). A step size of $2\theta = 0.01°$ was used over a 2θ range from 2.5 to 50° (see Figure S1 in the Supporting Information). The synthesized, activated material was determined to be UiO-66(Zr) by comparison to previously reported diffractograms.[49−52]

Gas adsorption isotherms of nitrogen (Praxair, 99.999%) adsorption at 77 K were obtained on a Micrometrics Gemini VII 2390 surface area and pore volume analyzer (see Figure S2 in the Supporting Information). The Brunauer–Emmett–Teller (BET) surface area in the relative pressure range of $0.05 < \frac{P}{P_0} < 0.3$ was determined to be 1280 ± 20 $m^2\ g^{-1}$, which is consistent with previous reports of modulated syntheses of UiO-66(Zr).[52,53] The pore surface area and volume as obtained from the t-plot using the Harkins and Jura equation[54] were 1180 ± 20 $m^2 g^{-1}$ and 0.60 ± 0.05 $cm^3\ g^{-1}$ respectively (see Figure S3 in the Supporting Information).

DOI: 10.1021/acs.jpcc.7b12628
J. Phys. Chem. C XXXX, XXX, XXX–XXX

The sizes of the UiO-66(Zr) crystallites and aggregates were approximated using field-emission scanning electron microscopy (Hitachi S-5000 FE-SEM) (see Figure S4 in the Supporting Information). All UiO-66(Zr) particles were mounted to SEM stubs using carbon tape and sputter coated with Au/Pd prior to imaging. A beam voltage of 10 kV was used for all images.

Sample Preparation in NMR Rotors. UiO-66(Zr) was packed into 3.2 mm outer diameter zirconia MAS rotors. Rotors were weighed prior to and after packing to determine the mass of the packed UiO-66(Zr). A microsyringe was used to add adsorbates (acetone (Sigma, 99%), methanol (Sigma, 99.5%), and cyclohexane (Sigma, 100%)) to the rotor, after which the rotor was capped and weighed again to determine the adsorbate mass. After adsorbate dosing, the rotor was heated to 323 K for 20 min to equilibrate and weighed again to ensure adsorbate containment within the rotor. Rotors were found to be liquid-tight, with no sample loss after the equilibration period. Samples were also weighed after the completion of experiments and determined to be liquid-tight over the timespan of the experiments performed. For control experiments without UiO-66(Zr), a rotor was filled with nonporous KBr and saturated with the neat adsorbate. This method was used to limit the amount of liquid in the rotor and thus ensure rotor stability.

NMR Experiments. All nuclear magnetic resonance (NMR) experiments were performed on a Bruker Avance spectrometer at a magnetic field strength of 16.4 T, corresponding to ^{1}H and ^{13}C Larmor frequencies of 700.13 and 176.04 MHz, respectively, with a Bruker narrow bore H/C/N magic angle spinning (MAS) probe. Experiments studying small molecule adsorption in UiO-66(Zr) were performed at a spinning rate of 5 kHz. Control experiments on neat adsorbates were performed at a 4 kHz spinning rate. Efforts were made to shim as best as possible on neat solvent samples, though some line shape imperfections remained at low intensity. ^{1}H adsorption experiments were performed using a spin echo ($90°-\tau-180°-\tau-$acquire) pulse sequence to eliminate the background signal from the NMR probe.[55] A radio frequency (RF) field strength (B_1) of 47 kHz and spin echo delay of τ = 200 μs were used in all ^{1}H NMR experiments, which were found to be quantitative with a recycle delay of 12 s. ^{1}H two-dimensional (2D) homonuclear exchange spectroscopy experiments[56] were performed on samples with adsorbate loadings where additional peaks (relative to the neat adsorbate) emerged. Mixing times ranging from 0.001 to 1 s were used. A brief recycle delay of 1 s was used in all 2D spectra to reduce the time necessary to collect the 200 t_1 increments. ^{13}C adsorption experiments were performed using a one-pulse (90°-acquire) pulse sequence with continuous wave (CW) proton decoupling to eliminate J-couplings.[55] A RF field strength of 31 kHz and recycle delay of 4 s were used in all ^{13}C spectra; the shortened recycle delay did not allow for quantitative analysis of the spectra. All proton and carbon chemical shifts were referenced externally to the proton peak and tertiary carbon peak of adamantane at 1.8 and 38.5 ppm (on the TMS scale) respectively[57] and conducted at room temperature (~298 K).

Kohn–Sham Density Functional Theory (DFT) Calculations. Gaussian09 software was used to perform NMR chemical shift calculations.[58] Structural data for UiO-66(Zr) were taken from literature single-crystal X-ray diffraction (SCXRD) studies.[51] $Zr_6O_4(OH)_4$ clusters were removed from initial NMR calculations since they are assumed not to contribute significantly to the nucleus independent chemical shift (NICS). Removal of these clusters decreased computational time and the size of the basis sets necessary for calculations with zirconium. NMR calculations were performed at the B3LYP level of theory, with a 6-31G(d) basis set, using the gauge independent atomic orbital (GIAO) method to calculate NMR shielding tensors.[59] "Banquo atoms," which are fictitious atoms with no electrons or nuclear charge, were employed as probe nuclei for the local magnetic field[35] as a function of position inside the tetrahedral and octahedral pore environments of UiO-66(Zr). The diagonalized chemical shielding tensor

$$\sigma_{\text{shielding}} = \begin{bmatrix} \sigma_{xx} & 0 & 0 \\ 0 & \sigma_{yy} & 0 \\ 0 & 0 & \sigma_{zz} \end{bmatrix}$$

was obtained for all linker and Banquo atoms. It is important to note that the chemical shielding tensor is not expressed in units of chemical shift, but the isotropic nucleus independent chemical shift (referred to as NICS) for each Banquo atom was calculated as follows: $\delta^{\text{iso}}_{\text{NICS}} = -\frac{1}{3}(\text{Tr}(\sigma_{\text{shielding}}) - \text{Tr}(\sigma_{\text{ref}}))$. The trace (Tr) of the tensors is the sum of the diagonal components and σ_{ref} is the diagonalized chemical shielding tensor of the reference atom. In this model, $\text{Tr}(\sigma_{\text{ref}}) = 0$ ppm.[59] Thus, $\delta^{\text{iso}}_{\text{NICS}} = -\frac{1}{3}(\text{Tr}(\sigma_{\text{shielding}}))$ for our calculations and reported values. Coordination of methanol and acetone to the metal-oxyhydroxy clusters of UiO-66(Zr) was modeled using a single metal-oxyhydroxy cluster where formate groups were substituted for terephthalate linkers to maintain charge balance. The geometry of the cluster (in the presence of the guest molecule) was optimized at the B3LYP level of theory with the basis set DGDZVP, which is large enough to accurately describe zirconium-containing molecules.[60] The gauge independent atomic orbital (GIAO) method was used to calculate NMR shielding tensors for all atoms. Geometry optimizations and NMR shielding tensor calculations were performed for neat acetone and methanol in the absence of the metal-oxyhydroxy cluster. The difference in the isotropic chemical shifts ($\Delta\delta_{\text{coordination}} = -\frac{1}{3}(\text{Tr}(\sigma_{\text{adsorbed}}) - \text{Tr}(\sigma_{\text{free}}))$ presents an approximation of the influence of coordination on the observed chemical shifts of the adsorbed guest molecules. Competing effects of NICS and coordination are discussed in the sections below.

RESULTS AND DISCUSSION

^{1}H and ^{13}C MAS NMR spectra for cyclohexane adsorbed into UiO-66(Zr) for a range of cyclohexane loadings are shown in Figure 2. For ^{1}H NMR spectra at low cyclohexane loadings (6% mass ratio), two peaks emerged, both at lower frequencies with respect to the peak of neat cyclohexane. At higher loadings (11 and 44%), a third peak emerged with a chemical shift identical to that of neat cyclohexane, indicating saturation of the MOF pores and filling of the void space between crystallites. Thus, the two peaks at emerging at 6% loading were assigned to "in-pore" cyclohexane, while the third emerging peak at 11% and 44% was assigned to "ex-pore" cyclohexane, with "in-pore" and "ex-pore" referring to the local environment of existing inside and outside of UiO-66(Zr) crystallites (see Table S1 in the

DOI: 10.1021/acs.jpcc.7b12628
J. Phys. Chem. C XXXX, XXX, XXX−XXX

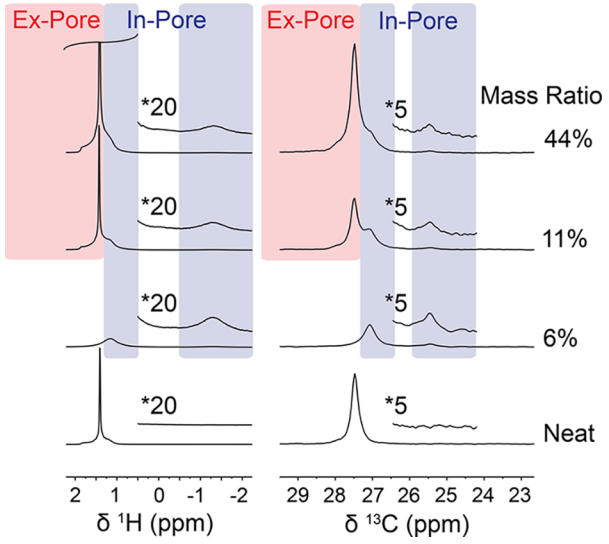

Figure 2. ^{1}H and ^{13}C NMR (16.4 T) spectra of cyclohexane subject to UiO-66(Zr) as a function of loading. The mass ratio is the (mass of cyclohexane used/mass of UiO-66(Zr) material). Amplifications of spectra are noted directly on the figure.

Supporting Information). Ex-pore adsorbate is assumed to occupy void space between the UiO-66(Zr) crystallites. We define the general formula specifying chemical shift deviation between in-pore and neat adsorbate as $\Delta\delta = \delta_{\text{in-pore}} - \delta_{\text{neat}}$, which gives values of −0.2 and −2.7 ppm here (corresponding to the two peaks in the 6% loading). Potential origins of the distinct in-pore environments are discussed below.

^{13}C experiments at both low and high loadings complemented ^{1}H experiments. At low loadings, two peaks emerged, both at lower frequencies relative to the peak of neat cyclohexane. At higher loadings, a third peak emerged, with a chemical shift equal to that of neat cyclohexane (see Table S1 in the Supporting Information). Both ^{1}H and ^{13}C resonances shifted in the same direction. The $\Delta\ \delta$ values were −0.4 and −2.1 ppm for ^{13}C NMR. 2D ^{1}H exchange spectroscopy experiments were performed for samples containing both in- and ex-pore resonances, though exchange between these environments could not be detected here due to the low intensity of the in-pore resonances.

Figure 3 shows comparable NMR results for acetone adsorbed into UiO-66(Zr). At low loadings (7.5 and 16% mass ratio), the broad peak associated with ^{1}H methyl protons resonated at lower frequencies compared to neat acetone. A second peak emerged at higher loadings (21, 40, and 63% mass ratio) at the same chemical shift of the methyl protons of the neat adsorbate (see Table S2 in the Supporting Information). Thus, the two peaks at low and high frequency were assigned to in- and ex-pore acetone, respectively. The proton $\Delta\delta$ for acetone takes a value of −0.5 ppm.

The ^{13}C carbonyl chemical shifts at low loadings (7.5 and 16% mass ratio) appeared at higher frequencies compared to the neat acetone carbonyl chemical shift (Figure 3). Similar to the ^{1}H experiments, a secondary carbonyl resonance emerged at higher loadings (21, 40, and 63% mass ratio), supporting the inference of pore saturation. The ^{13}C chemical shift of the second peak (at lower frequencies relative to the initial peak present at low loadings) matched the carbonyl chemical shift of the neat acetone (see Table S1 in the Supporting Information). The carbonyl peak presented a $\Delta\delta$ value of 2.5 ppm. Despite

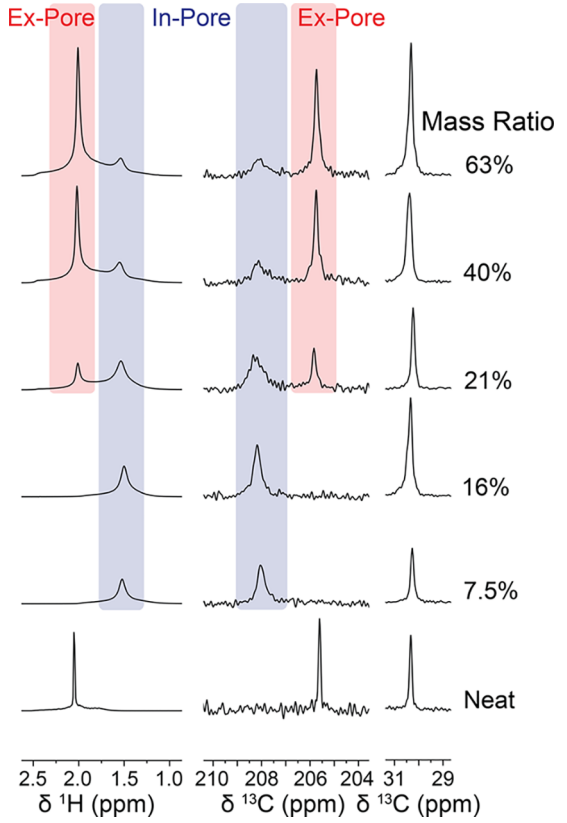

Figure 3. ^{1}H and ^{13}C NMR (16.4 T) spectra of acetone subject to UiO-66(Zr) as a function of loading. The mass ratio is the (mass of acetone used/mass of UiO-66(Zr) material).

the ^{1}H methyl NMR chemical shifts being sensitive to in- and ex-pore adsorbate, ^{13}C methyl chemical shifts were not significantly perturbed across multiple loadings, and thus distinct in- and ex-pore ^{13}C methyl resonances could not be identified. Contrary to cyclohexane, for which the ^{1}H and ^{13}C $\Delta\delta$ values have the same sign, acetone has ^{1}H and ^{13}C $\Delta\delta$ values of opposite sign. Furthermore, the lack of a change of chemical shift for the ^{13}C methyl group is possibly due to competing $\Delta\delta$ mechanisms, which are discussed below.

Qualitative inspection of peak line widths in Figure 3 suggests exchange between chemical environments. Thus, 2D ^{1}H homonuclear exchange spectroscopy experiments were performed to determine whether exchange occurred between the two resolved chemical environments assigned as in-pore and ex-pore acetone, and the time scale of said exchange. Cross-peak intensities at various mixing times (0.001, 0.1, and 0.5 s) demonstrate a chemical exchange time constant between the two environments on the order of hundreds of milliseconds (Figure 4).

The self-diffusion coefficient of neat acetone is reported to be 4.8×10^{-9} m^2s^{-1}.[61] In mesoporous materials such as silica, the self-diffusion coefficient of acetone has been demonstrated to be smaller in magnitude than the neat adsorbate self-diffusion coefficient, having a value of $\sim 10^{-10}$ m^2s^{-1}.[62] We surmise that this value may be reduced further in UiO-66(Zr) due to MOF-adsorbate interactions. The Einstein relation of the self-diffusion coefficient to root mean squared displacement (RMSD) of the molecule[63] was employed to qualitatively approximate the length scale associated with the observed chemical exchange process (t ∼ 100 ms).

DOI: 10.1021/acs.jpcc.7b12628
J. Phys. Chem. C XXXX, XXX, XXX−XXX

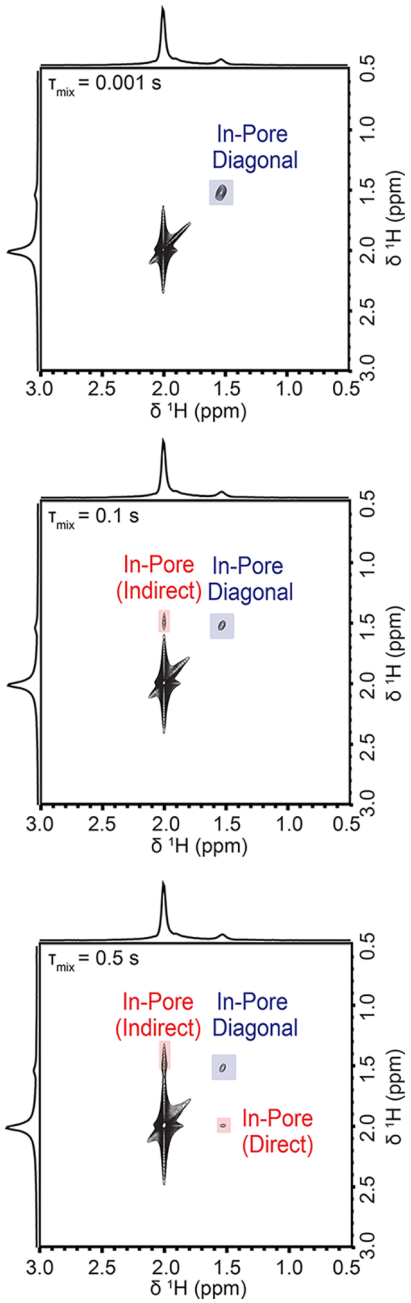

Figure 4. 2D homonuclear exchange spectroscopy experiments as a function of mixing time (0.001, 0.1, and 0.5 s). 40% acetone loading presented. First cross-peaks arise at ∼0.1 s.

$$\text{RMSD} = \sqrt{6Dt} = \sqrt{6 \times 10^{-10}\ \frac{\text{m}^2}{\text{s}} \times 0.1\ \text{s}} \times \frac{10^{-6}\mu\text{m}}{\text{m}}$$

$$\approx 10\ \mu\text{m}$$

This estimated length scale of the observed exchange was compared to the sizes of the crystals (∼nm) and particle conglomerates (∼μm) determined via field-emission scanning electron microscopy (FE-SEM) (see Figure S4 in the Supporting Information). The size of particle conglomerates was on the order of micrometers, qualitatively supporting the rationale that acetone could diffuse between the in- and ex-pore environments on the time scale of the exchange experiments.

Finally, the MAS NMR spectra of methanol adsorbed into UiO-66(Zr) were recorded to understand if the mechanism influencing the $\Delta\delta$ was consistent across various small molecules. Figure 5 demonstrates the ^{1}H and ^{13}C NMR spectra of methanol as a function of loading. At low loadings (22% mass ratio), the ^{1}H spectra exhibit only one prominent peak that is located at lower frequencies than the methyl proton resonance of neat methanol. This peak is assigned to in-pore methanol, and $\Delta\delta = -0.5$ ppm (see Table S3 in the Supporting Information). Upon further inspection, a significantly broadened peak is present around 4.5 ppm (see Figure S5 in the Supporting Information), which was assigned to the hydroxyl proton resonance of the in-pore adsorbate ($\Delta\delta = -0.3$ ppm). We note that the aromatic protons of the MOF appear at ∼7−8 ppm, and thus are not visible in the spectra presented in Figure 5.[64] At higher loadings (41, 66, and 90% mass ratio), two proton peaks (with chemical shifts similar to the hydroxyl and methyl groups of neat methanol) emerge and are assigned as ex-pore adsorbate (see Table S3 in the Supporting Information). Due to the broad nature of the ex-pore hydroxyl peak visible at higher loadings, the broadened in-pore hydroxyl resonance from the 22% mass ratio loading could no longer be clearly observed. 2D ^{1}H homonuclear exchange spectroscopy experiments tracking the methyl peak resonance were also performed at various mixing times (see Figure S6 in the Supporting Information), which revealed exchange between the in- and ex-pore methyl environments at a rate similar to acetone. Methanol in the fast limit of chemical exchange is also observed in spectra containing in- and ex-pore resonances.

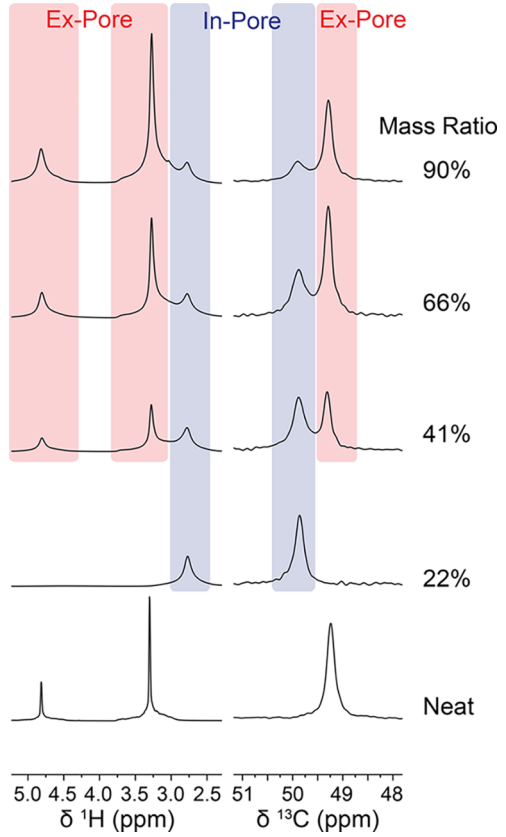

Figure 5. ^{1}H and ^{13}C NMR (16.4 T) spectra of methanol subject to UiO-66(Zr) as a function of loading. The mass ratio is the (mass of methanol used/mass of UiO-66(Zr) material).

DOI: 10.1021/acs.jpcc.7b12628
J. Phys. Chem. C XXXX, XXX, XXX−XXX

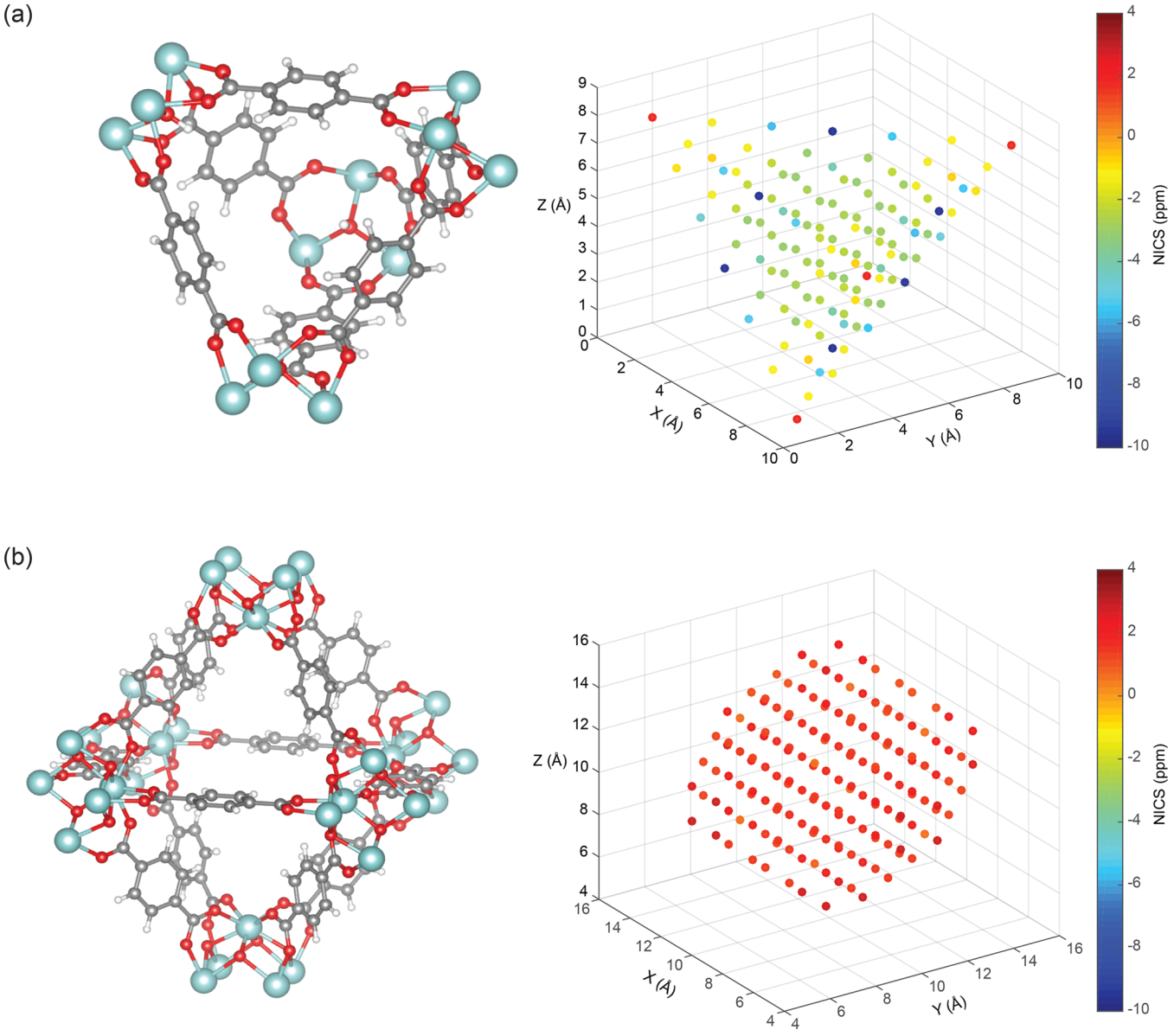

Figure 6. Nucleus independent chemical shifts (NICSs) as a function of position inside of the (a) tetrahedral (diameter = 8 Å) and (b) octahedral (diameter = 11 Å) pores of UiO-66(Zr).[11] The *X*, *Y*, and *Z* coordinates are arbitrary axes that define the coordinates of the pore.

^{13}C experiments at low loadings complemented ^{1}H experiments and also revealed in- and ex-pore resonances. In contrast to the ^{1}H spectral assignments, the peak at the higher frequency was determined to correspond to in-pore methanol, while the peak at the lower frequency corresponded to ex-pore methanol (see Table S3 in the Supporting Information). Similar to the $\Delta\delta$ values for ^{1}H and ^{13}C of acetone, the $\Delta\delta$ values for ^{1}H and ^{13}C of methanol had opposite signs. The origin of the observed changes of chemical shift are discussed below.

In summary, our NMR measurements have shown that different chemical shift changes are possible upon adsorption in UiO-66(Zr), with the observed shifts depending on the choice of adsorbate molecule as well as the studied nucleus. To account for these observations, three chemical shift deviation ($\Delta\delta$) mechanisms were considered: (i) ring-current shifts arising from the aromatic linkers in the framework, (ii) chemical shift changes due to coordination with Zr−OH moieties in the metal-oxyhydroxy cluster, and (iii) the effects of altering the self-solvation environment of the adsorbate.

We explored possible ring-current shifts by calculating nucleus independent chemical shifts (NICSs) for the tetrahedral and octahedral pores of UiO-66(Zr) (see the Supporting Information for Gaussian input files). The NICS gives a measure of the deviation in chemical shift that is anticipated upon adsorption due to sampling the local environment of MOF-linker ring-currents. The metal-oxy-hydroxy cluster was removed for these calculations due to its presumed negligible contribution to the conjugated system. Heat maps of the NICS as a function of position inside of the tetrahedral and octahedral pores are shown in Figure 6.

NICS calculations for the tetrahedral and octahedral pores were found to have $\Delta\delta$ of opposite signs, with the NICSs in the tetrahedral pore having predominantly negative value, and the NICSs in the octahedral pore having a predominantly positive value (Figure 6). This phenomenon (negative NICS above the plane of the conjugated system and positive NICS in the plane of the conjugated system) has been reported previously for simple conjugated systems.[34] Since DFT calculations are

DOI: 10.1021/acs.jpcc.7b12628
J. Phys. Chem. C XXXX, XXX, XXX−XXX

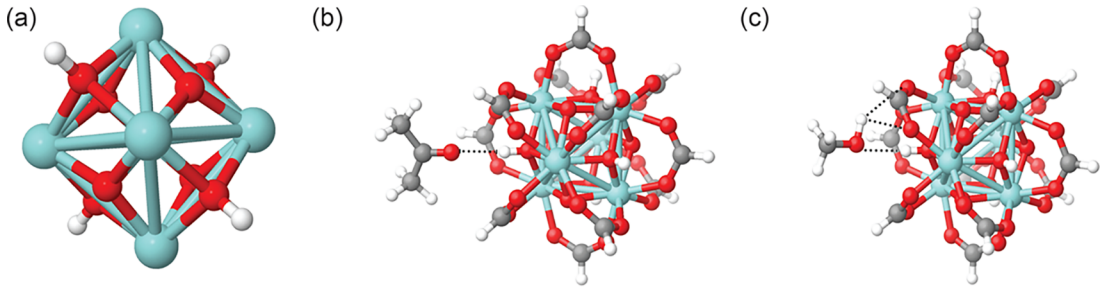

Figure 7. (a) Metal-oxyhydroxy cluster of UiO-66(Zr) composed of zirconium (blue), oxygen (red), and hydrogen (white). When activated at temperatures lower than 573 K, the metal-oxyhydroxy cluster contains Zr−OH moieties which can promote small molecule coordination. (b) Modeled coordination mode of acetone to formate-terminated metal-oxyhydroxy cluster. Dashed lines denote interatomic distances ≤ 2.5 Å. (c) Modeled coordination mode of methanol to formate-terminated metal-oxyhydroxy cluster. Dashed lines denote interatomic distances ≤ 2.5 Å.

performed at 0 K, these calculations assume that the linkers are immobile (terephthalate ring faces face into the tetrahedral pores, and sides face into the octahedral pores), and thus form an idealized system. Previous studies have demonstrated the mobility of the linkers at room temperature, which would reduce the magnitudes of the average NICS values in each pore relative to those calculated at 0 K.[65] Average NICS values do not account for the different regions of space that would be occupied by different nuclei. Further work would necessitate the assistance of MD and grand canonical Monte Carlo simulations, which may aid determination of portions of the pore accessible to certain atoms. Previous work on porous carbon materials has demonstrated the ability of MD simulations to parametrize regions of space accessible by various atoms of adsorbate molecules.[66]

NMR spectra for UiO-66(Zr) dosed with cyclohexane demonstrated two distinct in-pore resonances, both of which are shifted to lower frequencies relative to ex-pore resonances for both ^{1}H and ^{13}C NMR measurements (Figure 2). The similar shift changes for ^{1}H and ^{13}C appear consistent with NICS effects associated with ring currents. Both observed resonances are shifted to lower frequencies relative to ex-pore cyclohexane, suggesting that cyclohexane may favorably adsorb in the tetrahedral pores, based on NICS calculations (Figure 6), since cyclohexane cannot coordinate to the metal-oxyhydroxy clusters. This is in agreement with previous Monte Carlo simulations of cyclohexane in UiO-66(Zr).[12] In practice, we anticipate that cyclohexane undergoes dynamic exchange between the different positions within the octahedral and tetrahedral pores, and also exchange between these pores, so averaging of the chemical shift is expected. The average value of the calculated NICS was −2.8 ppm in the tetrahedral pore and 2.1 ppm in the octahedral pore. In one unit-cell of UiO-66(Zr), 1/3 of the volume arises from tetrahedral cage voids, and 2/3 from octahedral cage voids. Thus, if accounting for volume-weighted two-site exchange: $\delta_{\mathrm{NICS}}^{\mathrm{iso}} = \frac{1}{3} \times (-2.8$ ppm$) + \frac{2}{3} \times (2.1$ ppm$) \approx 0.5$ ppm. This further supports preferential tetrahedral pore adsorption, since all of the observed shift deviations for both ^{1}H and ^{13}C are negative for cyclohexane. It is not, however, immediately apparent why two distinct in-pore resonances should be observed for cyclohexane, as seen in both ^{1}H and ^{13}C spectra. One possible explanation is cyclohexane confined in two different conformations (boat and chair) that interconvert slowly and can thus be resolved, which results in two distinct chemical shifts. This, however, is unlikely, due to the uneven populations (and vastly different chemical shifts) of the two in-pore resonances (Figure 2). Furthermore, interconversion between boat and chair structures is likely to be in fast exchange on the NMR time scale at room temperature,[67] and thus isolated populations should not be observable. Another possible explanation is that these resonances arise from intracrystalline heterogeneity in the UiO-66(Zr) structure. Indeed, the synthesized UiO-66(Zr) material was measured to contain some defects, based on BET surface area characterization measurements (see Figure S2 in the Supporting Information). The use of modulators (including formic acid) has been demonstrated to introduce missing linker defects,[8,20,47,52,68−70] and previous studies have hypothesized these defects to be contained in correlated regions of the MOF.[46] We posit that the smaller NICS (−0.2 ppm for ^{1}H and −0.4 ppm for ^{13}C) may correspond to a defective region (fewer terephthalate linkers result in fewer ring currents to contribute to a negative NICS), whereas the larger NICS (−2.7 ppm for ^{1}H and −2.1 ppm for ^{13}C) may correspond to a region with more terephthalate linkers (fewer defects). Further investigation is, however, needed to confirm this hypothesis, including NMR measurements as a function of defect concentration.

In contrast to the NMR spectra for cyclohexane, the acetone and methanol NMR spectra show ^{1}H and ^{13}C $\Delta\delta$ values of opposite signs, rejecting the hypothesis of the NICS being the dominant mechanism of chemical shift deviation for these molecules. We considered that the Zr−OH in the metal-oxyhydroxy cluster (present for UiO-66(Zr) activated at temperatures below 573 K) (Figure 7a) may provide a coordination site for acetone and methanol, which could influence the $\Delta\delta$ value.[49] Proposed modes of adsorption of acetone (Figure 7b) and methanol (Figure 7c) are illustrated above, with hydrogen bonding interactions between the probe molecule and the Zr−OH group in each case.

Previous experimental and theoretical investigations of zeolites imbibed with acetone have successfully characterized the acidity (Lewis and Bronsted) of zeolites using ^{13}C chemical shift of acetone as a probe (since acetone coordinates to the −OH groups of the zeolite framework).[71−74] NMR spectroscopy of adsorbed acetone has unveiled structure−activity relationships of solid-acid catalysts.[74,75] Furthermore, computational and experimental studies have demonstrated that defects affect the acidity of UiO-66(Zr) materials.[76,77] Thus, we hypothesized that acetone and methanol could coordinate to the Zr−OH groups of the metal-oxyhydroxy clusters.

We calculated chemical shift deviations for small molecule coordination on model structures where the metal-oxyhydroxy

DOI: 10.1021/acs.jpcc.7b12628
J. Phys. Chem. C XXXX, XXX, XXX−XXX

cluster was terminated with formate groups. The difference in the chemical shifts between the coordinated acetone/methanol and neat acetone/methanol were attributed to the coordination of the guest molecule to the metal-oxyhydroxy cluster as determined by DFT. Tables 1 and 2 demonstrate the $\Delta\delta$ values

Table 1. Chemical Shift Deviation ($\Delta\delta$) of Resonances of Acetone

method	$\Delta\delta_{methyl}(^{13}C)$	$\Delta\delta_{carbonyl}(^{13}C)$	$\Delta\delta_{methyl}(^{1}H)$
exptl	0 ppm	2.5 ppm	−0.5 ppm
DFT	0.6 ppm	9.4 ppm	0.2 ppm

Table 2. Chemical Shift Deviation ($\Delta\delta$) of Resonances of Methanol

method	$\Delta\delta_{methyl}(^{13}C)$	$\Delta\delta_{methyl}(^{1}H)$	$\Delta\delta_{hydroxyl}(^{1}H)$
exptl	0.6 ppm	−0.5 ppm	−0.3 ppm
DFT	0.1 ppm	−0.1 ppm	1.1 ppm

as calculated by DFT and measured by experiment for both ^{1}H and ^{13}C for both acetone and methanol. For acetone coordination to the metal oxide cluster, the raw complexation energy was found to be −7.28 kcal mol^{-1}, as opposed to the −5.50 kcal mol^{-1} corrected complexation energy (accounting for basis set superposition error (BSSE)). For methanol coordination to the metal oxide cluster, the raw complexation energy was found to be −8.43 kcal mol^{-1}, as opposed to the −6.43 kcal mol^{-1} corrected complexation energy. Since BSSE mandates a 25% correction in the adsorption energies, we note that Tables 1 and 2 should be evaluated qualitatively.

Qualitatively, the positive $\Delta\delta$ value of the carbonyl ^{13}C resonance is in agreement with coordination of acetone to the metal-oxyhydroxy cluster. However, since DFT calculations are performed at 0 K with a static structural model, chemical shift deviations due to coordination are expected to be exaggerated by the calculations.[59] It is important to note that the presented DFT calculations are performed on a single adsorbate molecule, as opposed to a cluster of self-solvating adsorbate molecules inside of a cage (which is likely to be present experimentally). Experiments were carried out to quantify effect of removing the interactions provided by self-solvation (present in solution) that isolated molecules do not experience (see Figure S7 and Table S4 in the Supporting Information). This self-solvation was found to be an important factor in chemical shift deviations, and must be accounted for when comparing the chemical shift of an isolated molecule to that of the bulk solution. Removal of self-solvation effects (as would be experienced by dilute adsorbate in cyclohexane) have $\Delta\delta(^{1}H)$ values on the order of magnitude of the observed chemical shift deviations. However, due to the sizes of the MOF pores (tetrahedral diameter = 8 Å and octahedral diameter = 11 Å) and corresponding adsorbate kinetic diameters (4.6 Å for acetone and 3.6 Å for methanol),[78,79] full removal of self-solvation is unlikely. Further study must be carried out with MD or grand canonical Monte Carlo simulations to determine the extent of self-solvation removal inside of the pore environment. Previous computational studies have found that the effect of self-solvation on the calculated NICSs scale as $\frac{1}{3}\chi_m$, where χ_m is the magnetic susceptibility of the studied molecule.[80] Furthermore, computational studies using acetone and methanol in nanoporous materials (graphene slit pores) have demonstrated the ordering of solvent for polar molecule solvation shell stabilization, which reduces effective susceptibility to 5−10% of the bulk liquid contributions.[81]

The chemical shift deviation ($\Delta\delta$) of the methyl protons in acetone measured by experiment are the opposite sign to the methyl proton $\Delta\delta$ associated with Zr−OH coordination as calculated by DFT. This rejects the hypothesis that the negative $\Delta\delta$ of the methyl protons were caused solely by coordination. Thus, we hypothesize that there are three competing components to the variation of the in-pore chemical shift from the ex-pore chemical shift: $\Delta\delta = \Delta\delta_{coordination} + \Delta\delta_{self\text{-}solvation} + \delta^{iso}_{NICS}$. We infer that the dominant effect in acetone is coordination (though further efforts must deconvolute coordination from self-solvation), while the dominant effect in cyclohexane is the NICS.

DFT calculations on coordinated methanol were less conclusive. The calculated chemical shift changes appear much smaller than the observed experimental ones, and the value calculated for the hydroxyl group has the opposite sign to the experimental value. Altering of self-solvation may be partially responsible for this, due to the strong hydrogen bonding nature of methanol. As previously discussed, hydrogen bonding has been shown to be an important factor in chemical shift deviations, with the chemical shift varying as a function of hydrogen bond distance.[82−85] The modes of binding for methanol, a comparatively higher boiling point substance, are more complex than the modes for acetone and are a topic of further investigation to determine the dominant mechanism for chemical shift deviations for in-pore methanol. Current DFT calculations have simplified a periodic system into small clusters and future work will be performed with periodic calculations to reflect the nature of the experimental system with greater accuracy.

CONCLUSIONS

NMR spectroscopy has been used to probe the adsorption environments of guest molecules inside the MOF UiO-66(Zr). DFT calculations can inform the adsorption mechanisms present in the confined environments. We conclude the following:

(1) In- and ex-pore adsorbate resonances can be identified in UiO-66(Zr) by resolved peaks with different chemical shifts in both ^{1}H and ^{13}C NMR spectra for the guest molecule. Distinct in-pore resonances could be observed for cyclohexane, acetone, and methanol. Depending on the molecule and the studied nucleus, the chemical shift deviations upon adsorption ($\Delta\delta$) have different magnitude and signs.

(2) Three possible mechanisms for the different ($\Delta\delta$) values have been identified and explored by DFT calculations and experiments. First, ring-current effects associated with aromatic linkers can give rise to nucleus-independent chemical shifts. Second, some small molecules can bind with the Zr−OH groups on the metal-oxyhydroxy cluster, leading to chemical shift deviations upon coordination. Third, altering the solvating environment of adsorbate molecules that may hydrogen bond (self-solvation) can impact the chemical shift deviations.

(3) For UiO-66(Zr) loaded with cyclohexane, two in-pore resonances are observed in both ^{1}H and ^{13}C NMR, with similar $\Delta\delta$ values. This suggests that ring-current effects dominate the observed shift deviations for cyclohexane. The results suggest that cyclohexane preferentially adsorbs in the tetrahedral pores.

(4) For UiO-66(Zr) loaded with acetone and methanol, $\Delta\delta$ values with opposite signs are observed in ^{1}H and ^{13}C NMR experiments. This suggests that the ring currents of the organic

DOI: 10.1021/acs.jpcc.7b12628
J. Phys. Chem. C XXXX, XXX, XXX−XXX

linker are not the dominant factor contributing to the in-pore chemical environment, and that coordination at the Zr−OH moieties in combination with alteration of self-solvation significantly perturbs the chemical shifts.

We envision our work being used to advance understanding of catalytic MOFs as well as MOFs used for chemical capture and separation. This method can inform catalytic mechanisms of reactions occurring inside catalytic MOF materials by providing a method for identifying in-pore reactants and products. Quantitative ^{1}H NMR spectra can be used to determine consumption of in-pore reactant in reactions, thus generating a way to study reaction mechanisms inside of MOFs on the NMR time scale. Those same spectra can also be used to determine the saturation point of MOF materials. Analyzing the spectra of multiple NMR nuclei (in this case ^{1}H and ^{13}C) on the same guest molecule sheds light on the guest molecule's adsorption mechanism inside of the pore environment.

■ ASSOCIATED CONTENT

Supporting Information

The Supporting Information is available free of charge on the ACS Publications website at DOI: 10.1021/acs.jpcc.7b12628.

PXRD of synthesized UiO-66(Zr) material as compared to simulated diffractograms; BET isotherms of nitrogen adsorption for surface area determination; T-plot data for pore volume determination (Harkins and Jura); tabulated chemical shifts of acetone (neat, in-, and ex-pore); FE-SEM images of the synthesized UiO-66(Zr) material; tabulated chemical shifts of methanol (neat, in-, and ex-pore); zoomed in ^{1}H NMR spectrum with methanol loading (22%) demonstrating −OH in-pore peak; 2D ^{1}H homonuclear exchange experiments for methanol; tabulated chemical shifts of cyclohexane (neat, in-, and ex-pore); chemical shift analysis of adsorbate molecules without self-solvation interactions vs bulk adsorbate; quantitative analysis of pore filling via ^{1}H NMR of acetone; Gaussian NICS XYZ data; Gaussian adsorption XYZ data (PDF)

■ AUTHOR INFORMATION

Corresponding Authors

*E-mail: vjwitherspoon@berkeley.edu.
*E-mail: reimer@berkeley.edu.

ORCID

Aditya Nandy: 0000-0001-7137-5449
Alexander C. Forse: 0000-0001-9592-9821
Velencia J. Witherspoon: 0000-0002-2718-6605

Author Contributions

⊥V.J.W. and J.A.R.: Contributed equally to this work.

Notes

The authors declare no competing financial interest.

■ ACKNOWLEDGMENTS

This work was supported as part of the Center for Gas Separations Relevant to Clean Energy Technologies, an Energy Frontier Research Center funded by the U.S. Department of Energy, Office of Science, Basic Energy Sciences under Award # DE-SC0001015 (Experimental and Computational Studies). A.N. acknowledges a Regents' and Chancellor's Research Fellowship. A.C.F. thanks the Philomathia Foundation and Berkeley Energy and Climate Institute for funding. V.J.W. acknowledges the National Science Foundation under Award DGE # 1106400 and the College of Chemistry Chevron Graduate Research Fellowship. DFT calculations were performed on the computational cluster at the University of California Berkeley Molecular Graphics and Computation Facility (NIH Award # S10OD023532). We acknowledge Yusu Chen (U.C. Berkeley) for collecting powder x-ray diffraction data and Christopher Ho (U.C. Berkeley) for providing access to gas adsorption isotherm instrumentation. We also acknowledge Dr. Matthew Cliffe (University of Cambridge) and Dr. Miguel Gonzalez (U.C. Berkeley) for helpful discussions on UiO-66(Zr) synthesis. Lastly, we acknowledge Dr. Kathleen Durkin and Dr. Guangwei Min for assistance with computations and FE-SEM respectively.

■ REFERENCES

(1) Eddaoudi, M.; Kim, J.; Rosi, N.; Vodak, D.; Wachter, J.; O'Keeffe, M.; Yaghi, O. M. Systematic Design of Pore Size and Functionality in Isoreticular MOFs and their Application in Methane Storage. *Science* **2002**, *295*, 469−472.

(2) Furukawa, H.; Cordova, K. E.; O'Keeffe, M.; Yaghi, O. M. The Chemistry and Applications of Metal-Organic Frameworks. *Science* **2013**, *341*, 1230444.

(3) Lucier, B.; Zhang, Y.; Lee, K.; Lu, Y.; Huang, Y. Grasping Hydrogen Adsorption and Dynamics in Metal-Organic Frameworks Using ^{2}H Solid-State NMR. *Chem. Commun.* **2016**, *52*, 7541−7544.

(4) Chavan, S.; Vitillo, J. G.; Gianolio, D.; Zavorotynska, O.; Civalleri, B.; Jakobsen, S.; Nilsen, M. H.; Valenzano, L.; Lamberti, C.; Lillerud, K. P.; et al. H_2 Storage in Isostructural UiO-67 and UiO-66 MOFs. *Phys. Chem. Chem. Phys.* **2012**, *14*, 1614−1626.

(5) Van de Voorde, B.; Bueken, B.; Denayer, J.; De Vos, D. Adsorptive Separation on Metal-Organic Frameworks in the Liquid Phase. *Chem. Soc. Rev.* **2014**, *43*, 5766−5788.

(6) Nguyen, H. G. T.; Schweitzer, N. M.; Chang, C. Y.; Drake, T. L.; So, M. C.; Stair, P. C.; Farha, O. K.; Hupp, J. T.; Nguyen, S. T. Vanadium-Node-Functionalized UiO-66: A Thermally Stable MOF-Supported Catalyst for the Gas-Phase Oxidative Dehydrogenation of Cyclohexene. *ACS Catal.* **2014**, *4*, 2496−2500.

(7) Cavka, J. H.; Jakobsen, S.; Olsbye, U.; Guillou, N.; Lamberti, C.; Bordiga, S.; Lillerud, K. P. A New Zirconium Inorganic Building Brick Forming Metal-Organic Frameworks with Exceptional Stability. *J. Am. Chem. Soc.* **2008**, *130*, 13850−13851.

(8) Katz, M. J.; Brown, Z. J.; Colón, Y. J.; Siu, P. W.; Scheidt, K. A.; Snurr, R. Q.; Hupp, J. T.; Farha, O. K. A Facile Synthesis of UiO-66, UiO-67 and Their Derivatives. *Chem. Commun.* **2013**, *49*, 9449−9451.

(9) Ploskonka, A. M.; Marzen, S. E.; DeCoste, J. B. Facile Synthesis and Direct Activation of Zirconium Based Metal-Organic Frameworks from Acetone. *Ind. Eng. Chem. Res.* **2017**, *56*, 1478−1484.

(10) Ragon, F.; Horcajada, P.; Chevreau, H.; Hwang, Y. K.; Lee, U. H.; Miller, S. R.; Devic, T.; Chang, J. S.; Serre, C. *In-Situ* Energy-Dispersive X-Ray Diffraction for the Synthesis Optimization and Scale-Up of the Porous Zirconium Terephthalate UiO-66. *Inorg. Chem.* **2014**, *53*, 2491−2500.

(11) Moreira, M. A.; Santos, J. C.; Ferreira, A. F. P.; Loureiro, J. M.; Ragon, F.; Horcajada, P.; Shim, K. E.; Hwang, Y. K.; Lee, U. H.; Chang, J. S.; et al. Reverse Shape Selectivity in the Liquid-Phase Adsorption of Xylene Isomers in Zirconium Terephthalate MOF UiO-66f. *Langmuir* **2012**, *28*, 5715−5723.

(12) Duerinck, T.; Bueno-Perez, R.; Vermoortele, F.; De Vos, D. E.; Calero, S.; Baron, G. V.; Denayer, J. F. M. Understanding Hydrocarbon Adsorption in the UiO-66 Metal-Organic Framework: Separation of (Un)saturated Linear, Branched, Cyclic Adsorbates, Including Stereoisomers. *J. Phys. Chem. C* **2013**, *117*, 12567−12578.

(13) Ploskonka, A. M.; DeCoste, J. B. Tailoring the Adsorption and Reaction Chemistry of the Metal-Organic Frameworks UiO-66, UiO-66-NH_2, and HKUST-1 via the Incorporation of Molecular Guests. *ACS Appl. Mater. Interfaces* **2017**, *9*, 21579−21585.

DOI: 10.1021/acs.jpcc.7b12628
J. Phys. Chem. C XXXX, XXX, XXX−XXX

(14) Cmarik, G. E.; Kim, M.; Cohen, S. M.; Walton, K. S. Tuning the Adsorption Properties of UiO-66 via Ligand Functionalization. *Langmuir* **2012**, *28*, 15606−15613.
(15) Yang, D.; Bernales, V.; Islamoglu, T.; Farha, O. K.; Hupp, J. T.; Cramer, C. J.; Gagliardi, L.; Gates, B. C. Tuning the Surface Chemistry of Metal Organic Framework Nodes: Proton Topology of the Metal-Oxide-like Zr_6 Nodes of UiO-66 and NU-1000. *J. Am. Chem. Soc.* **2016**, *138*, 15189−15196.
(16) Trousselet, F.; Archereau, A.; Boutin, A.; Coudert, F.-X. Heterometallic Metal-Organic Frameworks of MOF-5 and UiO-66 Families: Insight from Computational Chemistry. *J. Phys. Chem. C* **2016**, *120*, 24885−24894.
(17) Wang, C.; Liu, X.; Chen, J. P.; Li, K. Superior Removal of Arsenic from Water with Zirconium Metal-Organic Framework UiO-66. *Sci. Rep.* **2015**, *5*, 16613.
(18) Ghosh, P.; Colón, Y. J.; Snurr, R. Q. Water Adsorption in UiO-66: The Importance of Defects. *Chem. Commun.* **2014**, *50*, 11329−11331.
(19) Vandichel, M.; Hajek, J.; Vermoortele, F.; Waroquier, M.; De Vos, D. E.; Van Speybroeck, V. Active Site Engineering in UiO-66 Type Metal-Organic Frameworks by Intentional Creation of Defects: a Theoretical Rationalization. *CrystEngComm* **2015**, *17*, 395−406.
(20) Liu, Y.; Klet, R. C.; Hupp, J. T.; Farha, O. Probing the Correlations between the Defects in Metal-Organic Frameworks and their Catalytic Activity by an Epoxide Ring-Opening Reaction. *Chem. Commun.* **2016**, *52*, 7806−7809.
(21) Borges, D. D.; Semino, R.; Devautour-Vinot, S.; Jobic, H.; Paesani, F.; Maurin, G. Computational Exploration of the Water Concentration Dependence of the Proton Transport in the Porous UiO-66(Zr)-$(CO_2H)_2$ Metal-Organic Framework. *Chem. Mater.* **2017**, *29*, 1569−1576.
(22) Ye, J.; Johnson, J. K. Design of Lewis Pair-Functionalized Metal Organic Frameworks for CO_2 Hydrogenation. *ACS Catal.* **2015**, *5*, 2921−2928.
(23) Na, K.; Choi, K. M.; Yaghi, O. M.; Somorjai, G. A. Metal Nanocrystals Embedded in Single Nanocrystals of MOFs Give Unusual Selectivity as Heterogeneous Catalysts. *Nano Lett.* **2014**, *14*, 5979−5983.
(24) Caratelli, C.; Hajek, J.; Cirujano, F.; Waroquier, M.; Llabrés i Xamena, F.; Van Speybroeck, V. Nature of Active Sites on UiO-66 and Beneficial Influence of Water in the Catalysis of Fischer Esterification. *J. Catal.* **2017**, *352*, 401−414.
(25) Kolokolov, D. I.; Maryasov, A. G.; Ollivier, J.; Freude, D.; Haase, J.; Stepanov, A. G.; Jobic, H. Uncovering the Rotation and Translational Mobility of Benzene Confined in UiO-66 (Zr) Metal-Organic Framework by the ^{2}H NMR-QENS Experimental Toolbox. *J. Phys. Chem. C* **2017**, *121*, 2844−2857.
(26) Ramsahye, N. A.; Gao, J.; Jobic, H.; Llewellyn, P. L.; Yang, Q.; Wiersum, A. D.; Koza, M. M.; Guillerm, V.; Serre, C.; Zhong, C. L.; et al. Adsorption and Diffusion of Light Hydrocarbons in UiO-66(Zr): A Combination of Experimental and Modeling Tools. *J. Phys. Chem. C* **2014**, *118*, 27470−27482.
(27) Trepte, K.; Schaber, J.; Schwalbe, S.; Drache, F.; Senkovska, I.; Kaskel, S.; Kortus, J.; Brunner, E.; Seifert, G. The Origin of the Measured Chemical Shift of ^{129}Xe in UiO-66 and UiO-67 Revealed by DFT Investigations. *Phys. Chem. Chem. Phys.* **2017**, *19*, 10020−10027.
(28) Chen, J. J.; Mason, J. A.; Bloch, E. D.; Gygi, D.; Long, J. R.; Reimer, J. A. NMR Relaxation and Exchange in Metal-Organic Frameworks for Surface Area Screening. *Microporous Mesoporous Mater.* **2015**, *205*, 65−69.
(29) Forse, A. C.; Griffin, J. M.; Merlet, C.; Carretero-Gonzalez, J.; Raji, A.-R. O.; Trease, N. M.; Grey, C. P. Direct Observation of Ion Dynamics in Supercapacitor Electrodes Using *In-Situ* Diffusion NMR Spectroscopy. *Nat. Energy* **2017**, *2*, 16216.
(30) Forse, A. C.; Griffin, J. M.; Wang, H.; Trease, N. M.; Presser, V.; Gogotsi, Y.; Simon, P.; Grey, C. P. Nuclear Magnetic Resonance Study of Ion Adsorption on Microporous Carbide-Derived Carbon. *Phys. Chem. Chem. Phys.* **2013**, *15*, 7722−7730.
(31) Moran, D.; Stahl, F.; Bettinger, H. F.; Schaefer, H. F.; Schleyer, P. v. R. Towards Graphite: Magnetic Properties of Large Polybenzenoid Hydrocarbons. *J. Am. Chem. Soc.* **2003**, *125*, 6746−6752.
(32) Kibalchenko, M.; Payne, M. C.; Yates, J. R. Magnetic Response of Single-Walled Carbon Nanotubes Induced by an External Magnetic Field. *ACS Nano* **2011**, *5*, 537−545.
(33) Brunklaus, G.; Koch, A.; Sebastiani, D.; Spiess, H. W. Selectivity of Guest-Host Interactions in Self-Assembled Hydrogen-Bonded Nanostructures Observed by NMR. *Phys. Chem. Chem. Phys.* **2007**, *9*, 4545−4551.
(34) Chen, Z.; Wannere, C. S.; Corminboeuf, C.; Puchta, R.; von Ragué Schleyer, P. Nucleus-Independent Chemical Shifts (NICS) as an Aromaticity Criterion. *Chem. Rev.* **2005**, *105*, 3842−3888.
(35) Forse, A. C.; Griffin, J. M.; Presser, V.; Gogotsi, Y.; Grey, C. P. Ring Current Effects: Factors Affecting the NMR Chemical Shift of Molecules Adsorbed on Porous Carbons. *J. Phys. Chem. C* **2014**, *118*, 7508−7514.
(36) Griffin, J. M.; Forse, A. C.; Tsai, W.-Y.; Taberna, P.-L.; Simon, P.; Grey, C. P. *In-Situ* NMR and Electrochemical Quartz Crystal Microbalance Techniques Reveal the Structure of the Electrical Double Layer in Supercapacitors. *Nat. Mater.* **2015**, *14*, 812−819.
(37) Forse, A. C.; Griffin, J. M.; Merlet, C.; Bayley, P. M.; Wang, H.; Simon, P.; Grey, C. P. NMR Study of Ion Dynamics and Charge Storage in Ionic Liquid Supercapacitors. *J. Am. Chem. Soc.* **2015**, *137*, 7231−7242.
(38) Yates, J. R.; Pham, T. N.; Pickard, C. J.; Mauri, F.; Amado, A. M.; Gil, A. M.; Brown, S. P. An Investigation of Weak CH-O Hydrogen Bonds in Maltose Anomers by a Combination of Calculation and Experimental Solid-State NMR Spectroscopy. *J. Am. Chem. Soc.* **2005**, *127*, 10216−10220.
(39) Uldry, A. C.; Griffin, J. M.; Yates, J. R.; Perez-Torralba, M.; Santa Maria, M. D.; Webber, A. L.; Beaumont, M. L. L.; Samoson, A.; Claramunt, R. M.; Pickard, C. J.; et al. Quantifying Weak Hydrogen Bonding in Uracil and 4-Cyano-4′-Ethynylbiphenyl: A Combined Computational and Experimental Investigation of NMR Chemical Shifts in the Solid State. *J. Am. Chem. Soc.* **2008**, *130*, 945−954.
(40) Zilka, M.; Sturniolo, S.; Brown, S. P.; Yates, J. R. Visualising Crystal Packing Interactions in Solid-State NMR: Concepts and Applications. *J. Chem. Phys.* **2017**, *147*, 144203.
(41) Li, J.; Li, S.; Zheng, A.; Liu, X.; Yu, N.; Deng, F. Solid-State NMR Studies of Host-Guest Interaction between UiO-67 and Light Alkane at Room Temperature. *J. Phys. Chem. C* **2017**, *121*, 14261−14268.
(42) Lacey, M. J.; Macdonald, C. G.; Pross, A.; Shannon, J. S.; Sternhell, S. Geminal Interproton Coupling Constants in Some Methyl Derivatives. *Aust. J. Chem.* **1970**, *23*, 1421−1429.
(43) Banwell, C. N.; Sheppard, N. High Resolution Nuclear Magnetic Resonance Spectra of Hydrocarbon Groupings. *Mol. Phys.* **1960**, *3*, 351−369.
(44) Hearmon, R. An Examination of the ^{13}C NMR Phenyl Substituent Effect in Branched and Non-Branched Alkyl Systems. *Org. Magn. Reson.* **1982**, *19*, 54−57.
(45) Watkins, M.; Olah, G. Study of Increasingly Crowded Phenylethanes by ^{13}C Spectroscopy and Molecular Mechanics Calculations. *J. Am. Chem. Soc.* **1981**, *103*, 6566−6574.
(46) Cliffe, M. J.; Wan, W.; Zou, X.; Chater, P. a.; Kleppe, A. K.; Tucker, M. G.; Wilhelm, H.; Funnell, N. P.; Coudert, F.-X.; Goodwin, A. L. Correlated Defect Nanoregions in a Metal-Organic Framework. *Nat. Commun.* **2014**, *5*, 4176.
(47) Hu, Z.; Castano, I.; Wang, S.; Wang, Y.; Peng, Y.; Qian, Y.; Chi, C.; Wang, X.; Zhao, D. Modulator Effects on the Water-Based Synthesis of Zr/Hf Metal-Organic Frameworks: Quantitative Relationship Studies between Modulator, Synthetic Condition, and Performance. *Cryst. Growth Des.* **2016**, *16*, 2295−2301.
(48) Yang, D.; Odoh, S. O.; Wang, T. C.; Farha, O. K.; Hupp, J. T.; Cramer, C. J.; Gagliardi, L.; Gates, B. C. Metal-Organic Framework Nodes as Nearly Ideal Supports for Molecular Catalysts: NU-1000-

DOI: 10.1021/acs.jpcc.7b12628
J. Phys. Chem. C XXXX, XXX, XXX−XXX

and UiO-66-Supported Iridium Complexes. *J. Am. Chem. Soc.* **2015**, *137*, 7391−7396.
(49) Valenzano, L.; Civalleri, B.; Chavan, S.; Bordiga, S.; Nilsen, M. H.; Jakobsen, S.; Lillerud, K. P.; Lamberti, C. Disclosing the Complex Structure of UiO-66 Metal-Organic Framework: A Synergic Combination of Experiment and Theory. *Chem. Mater.* **2011**, *23*, 1700−1718.
(50) Garibay, S. J.; Cohen, S. M. Isoreticular Synthesis and Modification of Frameworks with the UiO-66 Topology. *Chem. Commun.* **2010**, *46*, 7700−7702.
(51) Øien, S.; Wragg, D.; Reinsch, H.; Svelle, S.; Bordiga, S.; Lamberti, C.; Lillerud, K. P. Detailed Structure Analysis of Atomic Positions and Defects in Zirconium Metal-Organic Frameworks. *Cryst. Growth Des.* **2014**, *14*, 5370−5372.
(52) Shearer, G. C.; Chavan, S.; Ethiraj, J.; Vitillo, J. G.; Svelle, S.; Olsbye, U.; Lamberti, C.; Bordiga, S.; Lillerud, K. P. Tuned to Perfection: Ironing Out the Defects in Metal-Organic Framework UiO-66. *Chem. Mater.* **2014**, *26*, 4068−4071.
(53) Wu, H.; Chua, Y. S.; Krungleviciute, V.; Tyagi, M.; Chen, P.; Yildirim, T.; Zhou, W. Unusual and Highly Tunable Missing-linker Defects in Zirconium Metal-Organic Framework UiO-66 and Their Important Effects on Gas Adsorption. *J. Am. Chem. Soc.* **2013**, *135*, 10525−10532.
(54) Harkins, W. D.; Jura, G. Surfaces of Solids. XII. An Absolute Method for the Determination of the Area of a Finely Divided Crystalline Solid. *J. Am. Chem. Soc.* **1944**, *66*, 1362−1366.
(55) Keeler, J. *Understanding NMR Spectroscopy*; 2004; pp 8486.
(56) Aue, W. P.; Bartholdi, E.; Ernst, R. R. Two-Dimensional Spectroscopy. Application to Nuclear Magnetic Resonance. *J. Chem. Phys.* **1976**, *64*, 2229−2246.
(57) Morcombe, C. R.; Zilm, K. W. Chemical Shift Referencing in MAS Solid State NMR. *J. Magn. Reson.* **2003**, *162*, 479−486.
(58) Frisch, M.; Trucks, G.; Schlegel, H.; Scuseria, G.; Robb, M.; Cheeseman, J.; Scalmani, G.; Barone, V.; Mennucci, B.; Petersson, G. et al. *Gaussian09*, Revision B.01; Gaussian Inc., Pittsburgh, PA, 2010.
(59) Foresman, J. B.; Frisch, Æ. *Exploring Chemistry with Electronic Structure Methods*, 2nd ed.; Gaussian Inc.; Pittsburgh, PA, 1996; pp 266, 278−283.
(60) Holland, J. P.; Vasdev, N. Charting the Mechanism and Reactivity of Zirconium Oxalate with Hydroxamate Ligands using Density Functional Theory: Implications in New Chelate Design. *Dalton Trans.* **2014**, *43*, 9872−9884.
(61) McCall, D. W.; Douglass, D. C.; Anderson, E. W. Diffusion in Liquids. *J. Chem. Phys.* **1959**, *31*, 1555−1557.
(62) Kärger, J.; Valiullin, R. Diffusion in Porous Media. *eMagRes* **2011**, 1−14.
(63) Einstein, A. *Annalen der Physik* **1905**, *19*, 579.
(64) Devautour-Vinot, S.; Maurin, G.; Serre, C.; Horcajada, P.; Paula Da Cunha, D.; Guillerm, V.; De Souza Costa, E.; Taulelle, F.; Martineau, C. Structure and Dynamics of the Functionalized MOF Type UiO-66(Zr): NMR and Dielectric Relaxation Spectroscopies Coupled with DFT Calculations. *Chem. Mater.* **2012**, *24*, 2168−2177.
(65) Kolokolov, D. I.; Stepanov, A. G.; Guillerm, V.; Serre, C.; Frick, B.; Jobic, H. Probing the Dynamics of the Porous Zr Terephthalate UiO-66 Framework Using ^{2}H NMR and Neutron Scattering. *J. Phys. Chem. C* **2012**, *116*, 12131−12136.
(66) Merlet, C.; Forse, A. C.; Griffin, J. M.; Frenkel, D.; Grey, C. P. Lattice Simulation Method to Model Diffusion and NMR Spectra in Porous Materials. *J. Chem. Phys.* **2015**, *142*, 094701.
(67) Bovey, F. A.; Hood, F. P., III; Anderson, E. R.; Kornegay, R. L. NMR Study of Rotational Barriers and Conformational Preferences. II. d11-Cyclohexane. *J. Chem. Phys.* **1964**, *41*, 2041−2044.
(68) Shearer, G. C.; Chavan, S.; Bordiga, S.; Svelle, S.; Olsbye, U.; Lillerud, K. P. Defect Engineering: Tuning the Porosity and Composition of the Metal-Organic Framework UiO-66 via Modulated Synthesis. *Chem. Mater.* **2016**, *28*, 3749−3761.
(69) Morris, W.; Wang, S.; Cho, D.; Auyeung, E.; Li, P.; Farha, O. K.; Mirkin, C. A. Role of Modulators in Controlling the Colloidal Stability and Polydispersity of the UiO-66 Metal-Organic Framework. *ACS Appl. Mater. Interfaces* **2017**, *9*, 33413−33418.
(70) Trickett, C. A.; Gagnon, K. J.; Lee, S.; Gándara, F.; Bürgi, H. B.; Yaghi, O. M. Definitive Molecular Level Characterization of Defects in UiO-66 Crystals. *Angew. Chem., Int. Ed.* **2015**, *54*, 11162−11167.
(71) Li, S.; Pourpoint, F.; Trébosc, J.; Zhou, L.; Lafon, O.; Shen, M.; Zheng, A.; Wang, Q.; Amoureux, J.-P.; Deng, F. Host-Guest Interactions in Dealuminated HY Zeolite Probed by ^{13}C-^{27}Al Solid-State NMR Spectroscopy. *J. Phys. Chem. Lett.* **2014**, *5*, 3068−3072.
(72) Barich, D. H.; Nicholas, J. B.; Xu, T.; Haw, J. F. Theoretical and Experimental Study of the ^{13}C Chemical Shift Tensors of Acetone Complexed with Brønsted and Lewis Acids Chemical Shift Tensors of Acetone Complexes. *J. Am. Chem. Soc.* **1998**, *120*, 12342−12350.
(73) Fang, H.; Zheng, A.; Chu, Y.; Deng, F. ^{13}C Chemical Shift of Adsorbed Acetone for Measuring the Acid Strength of Solid Acids: A Theoretical Calculation Study. *J. Phys. Chem. C* **2010**, *114*, 12711−12718.
(74) Zheng, A.; Li, S.; Liu, S. B.; Deng, F. Acidic Properties and Structure-Activity Correlations of Solid Acid Catalysts Revealed by Solid-State NMR Spectroscopy. *Acc. Chem. Res.* **2016**, *49*, 655−663.
(75) Haw, J. F.; Nicholas, J. B.; Xu, T.; Beck, L. W.; Ferguson, D. B. Physical Organic Chemistry of Solid Acids: Lessons from *In-Situ* NMR and Theoretical Chemistry. *Acc. Chem. Res.* **1996**, *29*, 259−267.
(76) Ling, S.; Slater, B. Dynamic Acidity in Defective UiO-66. *Chem. Sci.* **2016**, *7*, 4706−4712.
(77) Klet, R. C.; Liu, Y.; Wang, T. C.; Hupp, J. T.; Farha, O. K. Evaluation of Brønsted Acidity and Proton Topology in Zr- and Hf-Based Metal-Organic Frameworks using Potentiometric Acid-Base Titration. *J. Mater. Chem. A* **2016**, *4*, 1479−1485.
(78) Kajiwara, T.; Higuchi, M.; Yuasa, A.; Higashimura, H.; Kitagawa, S. One-Dimensional Alignment of Strong Lewis Acid Sites in a Porous Coordination Polymer. *Chem. Commun.* **2013**, *49*, 10459−10461.
(79) Borjigin, T.; Sun, F.; Zhang, J.; Cai, K.; Ren, H.; Zhu, G. A Microporous Metal-Organic Framework with High Stability for GC Separation of Alcohols from Water. *Chem. Commun.* **2012**, *48*, 7613−7615.
(80) Dračínsky, M.; Bouř, P. Computational Analysis of Solvent Effects in NMR Spectroscopy. *J. Chem. Theory Comput.* **2010**, *6*, 288−299.
(81) Terrones, J.; Kiley, P. J.; Elliott, J. A. Enhanced Ordering Reduces Electric Susceptibility of Liquids Confined to Graphene Slit Pores. *Sci. Rep.* **2016**, *6*, 26406.
(82) Wagner, G.; Pardi, A.; Wüthrich, K. Hydrogen Bond Length and Proton NMR Chemical Shifts in Proteins. *J. Am. Chem. Soc.* **1983**, *105*, 5948−5949.
(83) Wei, Y.; McDermott, A. E. Modeling NMR Chemical Shifts. *ACS Symp. Ser.* **2012**, *732*, 177−193.
(84) Hori, S.; Yamauchi, K.; Kuroki, S.; Ando, I. Proton NMR Chemical Shift Behavior of Hydrogen-Bonded Amide Proton of Glycine-Containing Peptides and Polypeptides as Studied by *Ab Initio* MO Calculation. *Int. J. Mol. Sci.* **2002**, *3*, 907−913.
(85) Zheng, G.; Wang, L.; Hu, J.; Zhang, X.; Shen, L.; Ye, C.; Webb, G. A. Hydrogen Bonding Effects on the ^{13}C NMR Chemical Shift Tensors of Some Amino Acids in the Solid State. *Magn. Reson. Chem.* **1997**, *35*, 606−608.

DOI: 10.1021/acs.jpcc.7b12628
J. Phys. Chem. C XXXX, XXX, XXX−XXX